The SuperCOSMOS data processing guides: Photometry

N C Hambly

June 2, 1998

Contents

1 Introduction **3**

2 Instrumental magnitudes **3**

3 Colour terms **4**

4 Instrumental magnitude scales of stars and galaxies **6**

5 Calibration **6**
5.1 Setting up the sequence 6
5.2 Galaxy magnitude calibration 8
5.3 Stellar magnitude calibration 10

6 External accuracy of calibrated photographic data **11**
6.1 Photometric field effects 12
6.2 Sky normalisation 13

7 Linearised instrumental magnitudes **18**

1 Introduction

In principle it is possible to achieve accuracies of up to $\sim 5\%$ when photometering well exposed images on a photographic plate (although the errors inevitably rise steeply towards the plate limits). In practice, random errors can often be dominated by systematics unless great care is taken when applying calibrations over the large areas of Schmidt plates and to differing image profiles. This guide describes the magnitude parameters available for each image, how they are derived, and also goes on to demonstrate various methods for calibrating the instrumental magnitudes onto the familiar apparent magnitude scale, including a discussion of colour terms and demonstration of typical 'field effects', or systematic errors.

2 Instrumental magnitudes

SuperCOSMOS measures *transmission* values for pixels in a photographic image whereas astronomers are generally interested in the relative intensity of objects, usually as described by the magnitude scale

$$\mathrm{m_2 - m_1 = -2.5\log(I_2/I_1)}.$$

The relationship between transmission of an image pixel and the total incident flux is somewhat complex. Photographers work in *density* units, where the density D is related to intensity I via (for example, James 1977)

$$\mathrm{D} = \gamma \log \mathrm{I},$$

where, for a science–grade scientific emulsion, this relationship is linear over ~ 3D (*e.g.* Scientific Imaging with Kodak Films and Plates, Kodak publication No. P–315) while a typical survey–grade Schmidt plate has $\gamma \sim 2.5$. The relationship between density and transmission is, by definition

$$\mathrm{D} = \log_{10}(\mathrm{T_C/T}),$$

where $\mathrm{T_C}$ is the transmission measured through clear air (or more strictly speaking through unexposed but developed emulsion). Hence, there is a non–linear relationship between T and I; moreover other non–linearities (*e.g.* saturation effects at high intensity, chemical fog at low intensity, and scattered light and/or diffraction in the imaging system during scanning) compound this non–linearity. Therefore, a transmission–to–intensity look–up table is used after scanning to provide a translation of pixel transmissions to relative intensities. In principle this LUT can be derived by measuring the step–wedge (if available) on the side of each plate which has spots of known relative intensity, but the measurement of a solid block of exposed emulsion at a given intensity is not generally applicable to small, dense images in an otherwise light emulsion (for example because of scattered light) so a calibration of the form $\log_{10}\mathrm{I} \propto \gamma^{-1}\log_{10}(1/\mathrm{T})$ is used for plate measurements, where $\gamma^{-1} = 0.3$ is assumed for a fine–grained emulsion on a survey–grade plate.

There are three parameters provided for each image image in the IAM file (see the introductory guide and the beginner's guide) that are relevant to image brightness. These are:

Param. #	Name	Description	Units
8	IPEAK	Brightest intensity above sky	intensity
9	COSMAG	$-2.5\log_{10}$(summed intensity)	millimags
10	ISKY	Sky intensity at centroid	intensity

The COSMAG parameter is an isophotal magnitude calculated as the summed intensity above sky of all pixels brighter than the threshold used to process the pixel data:

$$\mathrm{COSMAG} = \{-2.5\log_{10}\sum_{i=1}^{i=n}(I_i - I_{\mathrm{SKY}})\} \times 1000$$

for the n pixels above the threshold. Despite saturation effects and the limited dynamic range of the imaging system, increasingly brighter images have larger summed intensities due to growth in image size and there is a monotonically increasing relationship (albeit non–linear) between the instrumental and apparent magnitude scales.

It is worth mentioning several systematic effects in the instrumental magnitude scale at this point. Because the single T–to–I scale used is non–linear, any sensitivity variations across the field will result in stars with the same brightness having slightly different summed intensities depending on their positions within the field. The design of the UK Schmidt Telescope yields an unvignetted radius of $\sim 2.7°$ about the plate centre (Tritton 1983) while differential desensitisation of the emulsion due to moisture is minimised during exposure by dry nitrogen flushing. These result in a fairly uniform sensitivity across the unvignetted part of the plate; nevertheless, systematics of 10% to 20% can easily still be present. Also, thresholding can lead to systematic effects in the faintest objects where noise makes measured magnitudes too bright while extended wings of profiles below the threshold are lost. Finally, stars and galaxies are likely to have different instrumental magnitude scales since the integrated intensity of a diffuse object will change at a different rate relative to stars as the latter are more prone to saturation effects due to their steeper profiles. This means that the instrumental magnitudes of stars and galaxies must be treated separately (see later).

3 Colour terms

When compared to modern photoelectric devices, the combination of photographic emulsions and glass filters produce a different response to the spectral energy distributions of astronomical targets. For those objects having extreme colour, the effective wavelength of the photographic bandpass can be markedly different to the standard passband. This leads to colour terms between photoelectric and photographic systems. The following colour equations are taken from Blair & Gilmore (1982), Bessell (1979;1986) and Evans (1989) where more details can be found. The largest differences are observed for the $\mathrm{B_J}$ and $\mathrm{R_F}$ passbands, which are very different to their photoelectric counterparts — see, for example, Figure 11 of Evans (1989) and Figure 1 of Bessell (1986).

For the bands detailed in Table 1 (Johnson UBV; Cousins $\mathrm{R_C I_C}$) the following relationships are quoted:

$$\mathrm{U_{1O} = U - (0.03 \pm 0.05) \times (U - B); -0.4 \leq (U - B) \leq 2.0}$$

$$\mathrm{O = B + (0.135 \pm 0.03) \times (B - R_C); +0.5 \leq (B - R_C) \leq 2.5}$$

$$\mathrm{B_{38O} = B - (0.11 \pm 0.02) \times (B - V); -0.1 \leq (B - V) \leq 1.6}$$

$$\mathrm{B_J = B - (0.28 \pm 0.04) \times (B - V); -0.1 \leq (B - V) \leq 1.6}$$

$$\mathrm{V_{49D} = V - (0.10 \pm 0.02) \times (B - V); -0.1 \leq (B - V) \leq 1.6}$$

$$\mathrm{E = R_C + (0.00 \pm 0.02) \times (B - R_C); +0.7 \leq (B - R_C) \leq 2.7}$$

$$\mathrm{R_{59F} = R_C - 0.006 - 0.059 \times (R - I) + 0.112 \times (R - I)^2 + 0.0238 \times (R - I)^3}$$

Photoelectric passband	Emulsion	Filter	Photographic passband	Reference
U	IIa–O	UG1	U_{1O}	1
B	103a–O	none	O	2
	IIa–O	GG385	B_{38O}	1
	IIIa–J	GG395	B_J	1
V	IIa–D	GG495	V_{49D}	1
R_C	103a–E	2444	E	2
	IIIa–F	OG590	R_{59F}	3
	IIIa–F	RG630	R_{63F}	3
I_C	IV–N	RG715	I_N	3

References:
1: Blair & Gilmore (1982)
2: Evans (1989)
3: Bessell (1986)

Table 1: Photometric passbands defined by various emulsion/filter combinations

$$R_{63F} = R_C - 0.013 - 0.204 \times (R - I) + 0.1 \times (R - I)^2 + 0.0295 \times (R - I)^3$$

$$(R_{59F} - I_N) = -0.005 + 0.934(R - I) + 0.095(R - I)^2 + 0.034(R - I)^3$$

$$(R_{63F} - I_N) = -0.016 + 0.785(R - I) + 0.121(R - I)^2 + 0.027(R - I)^3$$

where $(R - I) = 0.965(R_C - I_C)$ and $(R_C - I_C) < 2.0$ — see Bessell (1986) for more details.

For example, the following code uses the above relationships to 'naturalise' a set of photoelectric BR magnitudes to B_J to allow calibration of instrumental magnitudes from a IIIaJ plate containing the same objects (see the following Sections):

```
      program makeseq
      implicit none
      real b,eb,bmr,vmr,bmv,bj
      character line*58

      open (unit=1,file='f4112.ccd',status='old',readonly)
      open (unit=2,file='sequence.dat',status='new')

10    read (1,'(a58,f6.3,f7.4,f7.3)',end=20) line,b,eb,bmr
      if (bmr.lt.1.5) vmr=0.358*bmr
      if (bmr.ge.1.5) vmr=0.35*bmr
      bmv=bmr-vmr
      bj=b-0.28*bmv
      write (2,'(a58,2f7.3)') line,bj,b
      goto 10
20    continue
      close (1)
      close (2)
      end
```

Note that the procedure of naturalising the calibrating magnitudes before comparing with instrumental magnitudes will reduce the scatter between the two measurements, particularly for stars of extreme colour when using J or R plates. Note also the use of the following relationships between (V–R) and (B–R) which were derived from photoelectric standards in the Graham Equatorial Regions (Hatzidimitriou, Hawkins & Gyldenkerne 1989):

$$(\mathrm{V}-\mathrm{R}) = (0.358 \pm 0.004) \times (\mathrm{B}-\mathrm{R}), (\mathrm{B}-\mathrm{R}) < 1.5;$$

$$(\mathrm{V}-\mathrm{R}) = (0.350 \pm 0.002) \times (\mathrm{B}-\mathrm{R}), (\mathrm{B}-\mathrm{R}) \geq 1.5.$$

Such relationships are useful when colour corrections are only available in terms of one colour [in this case (B–V)], another colour being measured [here, (B–R)]; note however that assumptions such as this are not necessarily valid for galaxies.

Once a set of 'standards' has been set up for a given field, it is possible to calibrate the instrumental magnitude onto a true apparent magnitude scale. The following Sections demonstrate and discuss this procedure.

4 Instrumental magnitude scales of stars and galaxies

As stated previously, due to the vagaries of the photographic and measurement processes, the instrumental magnitude scales of stars and galaxies will be different when compared to a true magnitude scale, *e.g.* calibration of galaxy instrumental magnitudes using a stellar sequence, or *vice versa*, will produce erroneous results. Figure 1 shows some example data where the SuperCOSMOS instrumental magnitude is plotted versus naturalised photoelectric magnitude in UKST field 411 at the SGP. The scales clearly diverge around 2.5 magnitudes above the detection limit — the galaxy scale is 'better behaved' (the relationship is more closely linear). The correct procedure for calibrating the scales is to use star/galaxy separated data (see the star/galaxy separation guide), and treat the two types of objects with independent calibrations (see the following two Sections).

5 Calibration

5.1 Setting up the sequence

The first step in calibration of instrumental magnitudes is to generate a sequence of standards from a source of photoelectric photometry. In the following example, CCD data were available and these were supplemented with brighter standards from the TYCHO catalogue. All stellar magnitudes were naturalised to $\mathrm{B_J}$ before calibration (see Section 3). The example code `nseq` searches an IAM file for every sequence star in a given file within a given search radius, then outputs a binary file of pointers to any images located. The code also produces a file `logfile` indicating the number of stars within the search radius for each sequence object (see the beginner's guide for more details):

```
% nseq
Input file containing coords & mags:
fullseq.dat
Equinox (0=1900, 1=1950, 2=J2000)
1
```

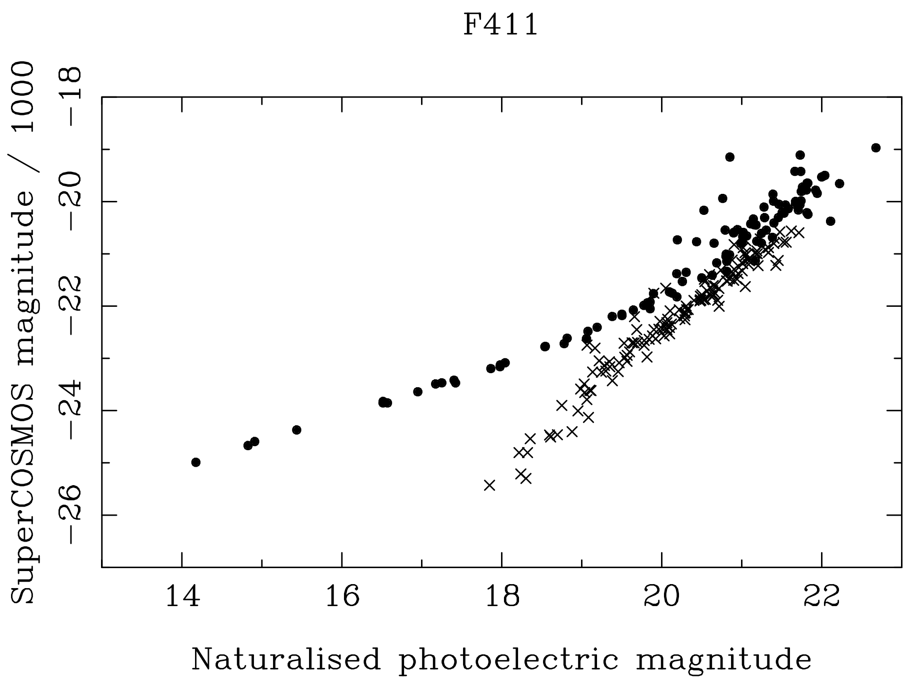

Figure 1: Stellar and galaxian instrumental magnitude scales (crosses are galaxies) when compared with naturalised photoelectric measures.

```
Start decoding sexagesimal co-ordinates at which character?
60
IAM file to be searched
/harv2/scos/skysurvey/UKJ411/iam.srtrd
Search radius (arcsec):
1.5
Output index file:
fullseq.idx
No. of sequence stars to search for:      305
%
```

The following points should be noted:

- The program is generalised to read each line in the sequence file as a character string, so that any name characters or other information before the co-ordinates can be skipped over; note also that co-ordinate strings should always be read as character strings in FORTRAN since an integer or floating point formatted read of `-0` would be read as `+0` (this is important for DECs between the equator and $-1°$).
- The co-ordinates in the sequence file can be at equinox 1900.0, B1950.0 or J2000.0; if not J2000.0 the code precesses the co-ordinates to this equinox before comparing with those in the IAM file (which are at equinox J2000.0)
- The search radius should be set given the accuracy of the co-ordinates in the input list. The logfile indicates if there is more than one possible match for an object (the nearest is chosen).

For speed and efficiency, the output index file is simply a binary file of integer pointers to records in the IAM file where images have been located. To inspect this file, use the unix command

```
% od -t d4 -v fullseq.idx | more
```

(see the introductory guide for information concerning `od` command line options). Any object in the input file that fails to be located in the IAM file has a pointer of zero written to the output index so that subsequent programs can ignore them. Once a sequence pointer file has been set up, calibration can take place.

5.2 Galaxy magnitude calibration

The example code `galcal` provides a means for calibrating galaxy magnitudes. The user is prompted for the order of fit for a polynomial (either 2 or 3, *i.e.* linear or quadratic) and then an iterative linear least–squares fit is applied to the standard magnitudes versus the instrumental magnitudes. A plot (see Figure 2) is produced showing the shape of the calibration and its residuals. The code finally makes a copy of the input file with all galaxy magnitudes calibrated, the calibrated magnitude being written to the spare IAM parameter number 32 in units of millimags:

```
% galcal
File containing naturalised sequence magnitudes:
fullseq.dat
Skip to which character to get required magnitude:
60
File containing index of pointers to the IAM file:
fullseq.idx
IAM file:
/harv2/scos/skysurvey/UKJ411/iam.srtrd
Normalise instrumental magnitudes to sky level (y/n)?
y
Output IAM file:
/disk1/nch/iam.srtrd.galcal
Order of fit (2 or 3, ie. linear or quadratic):
3
Graphics device/type (? to see list, default xwindows):
xwindows
No. of calibrating galaxies input:     140
No. of calibrating galaxies used for fit:      130
No. of records read from input IAM file:   293222
No. of galaxies calibrated:     48214
%
```

Once again, lines from the sequence file are read as character strings and the position of the relevant magnitude must be specified. Note that because the galaxy instrumental magnitude scale is approximately linear with unit gradient (when divided by 1000), in the absence of a photoelectric sequence the relative galaxy magnitudes may be determined using $\Delta m_{12} \approx (\mathrm{COSMAG}_1 - \mathrm{COSMAG}_2)/1000$. Normalisation of the instrumental magnitudes to the sky background level is recommended for deep survey plates when doing galaxy photometry — this subject is discussed in a little more detail in Section 6.2. For more information on photographic

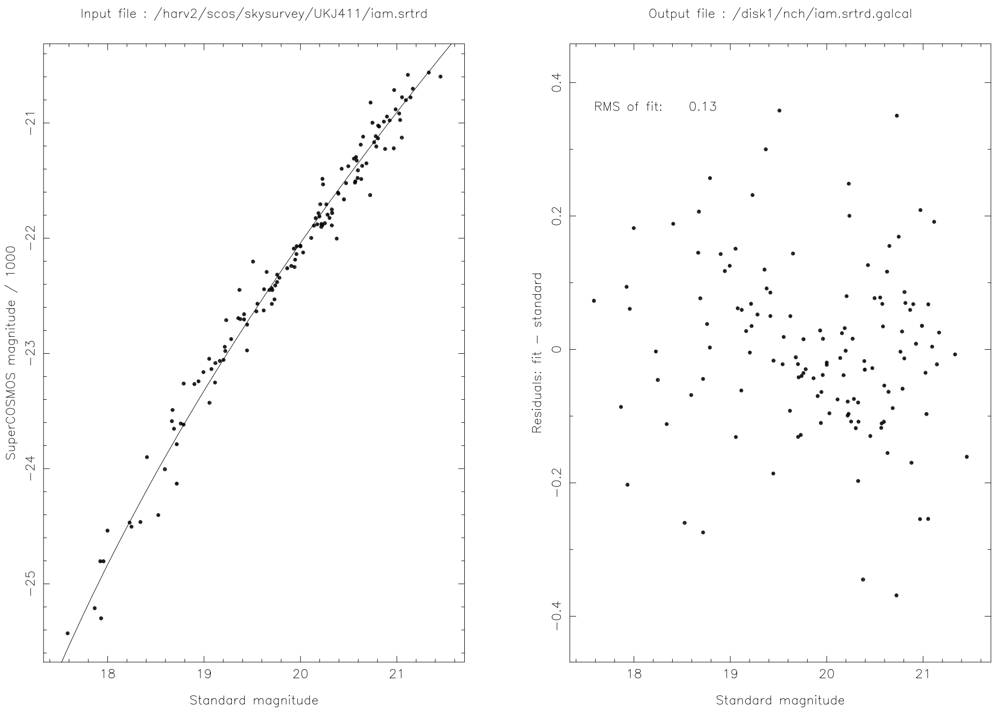

Figure 2: Output plot from code **galcal**. The left–hand panel shows the shape of the fitted least–squares polynomial along with the data after iteration. The right–hand panel shows the residuals as a function of magnitude, and the overall RMS of the fit.

photometry of galaxies from measuring machine data see Metcalfe, Fong & Shanks (1995) and references therein.

5.3 Stellar magnitude calibration

Figure 3 shows the relationship between the instrumental magnitude and real apparent magnitude for stars on a typical sky survey plate. Clearly, the instrumental magnitude scale is non–linear when compared with the true scale; this makes calibration by a single polynomial difficult since there are at least two closely linear portions in the range $8 < m < 14$ and $14 < m < 20$. A polynomial of sufficiently high order to model this shape would be unconstrained at the ends and would, more often than not, produce strange results at the faint extremes of colour–magnitude diagrams for example. A better approach is to use least–squares cubic spline pieces — this is implemented in the code `starcal` as detailed below. Again, a photometric sequence, and corresponding index (produced by the code `nseq`) are required. The user is then prompted for the number of 'knots' required for the spline model (this is one less than the number of spline pieces). The knots are spaced evenly in the interval containing calibration data, and the number is restricted to lie between 0 (which is equivalent to a single least–squares cubic polynomial fit) and 3. When calibration data are available over a large range, 2 or 3 knots are recommended; when only a restricted calibration sequence is available, 1 or 2 knots is usually a good choice. In general, 2 knots will produce good results, but some experimentation may be necessary depending on the available sequence data. Note that outside the range of the data, the calibration is linearly extrapolated. This is of course dangerous, and the calibration should not be trusted outside the range of the standards, but at least this procedure avoids the wildly unconstrained behaviour of even a relatively low–order polynomial. Note also that if not enough data are available for the specified number of knots and their placement, the program will report this and suggest running again with a reduced number of knots. A plot is produced showing the calibration curve and the residuals of the standards about the fit (see Figure 3). Finally, a new IAM file is created with each image having parameter 32 changed to the calibrated apparent magnitude in units of millimags. The code will calibrate all images if requested to do so, or only stars if star/galaxy separation flags are available — *e.g.* the procedure outlined in Section 5.2 can be executed to first calibrate the galaxies and write a temporary file; subsequently this code may be run to calibrate the stars (and also those images too faint for classification) and create a final, fully calibrated file as in the following example:

```
% starcal
File containing naturalised sequence magnitudes:
fullseq.dat
Skip to which character to get required magnitude:
60
File containing index of pointers to the IAM file:
fullseq.idx
IAM file:
/disk1/nch/iam.srtrd.galcal
Normalise instrumental magnitudes to sky level (y/n)?
n
Output IAM file:
/disk1/nch/iam.srtrd.stargalcal
Number of knots? Maximum = :       3
(0 = least-squares cubic polynomial)
2
```

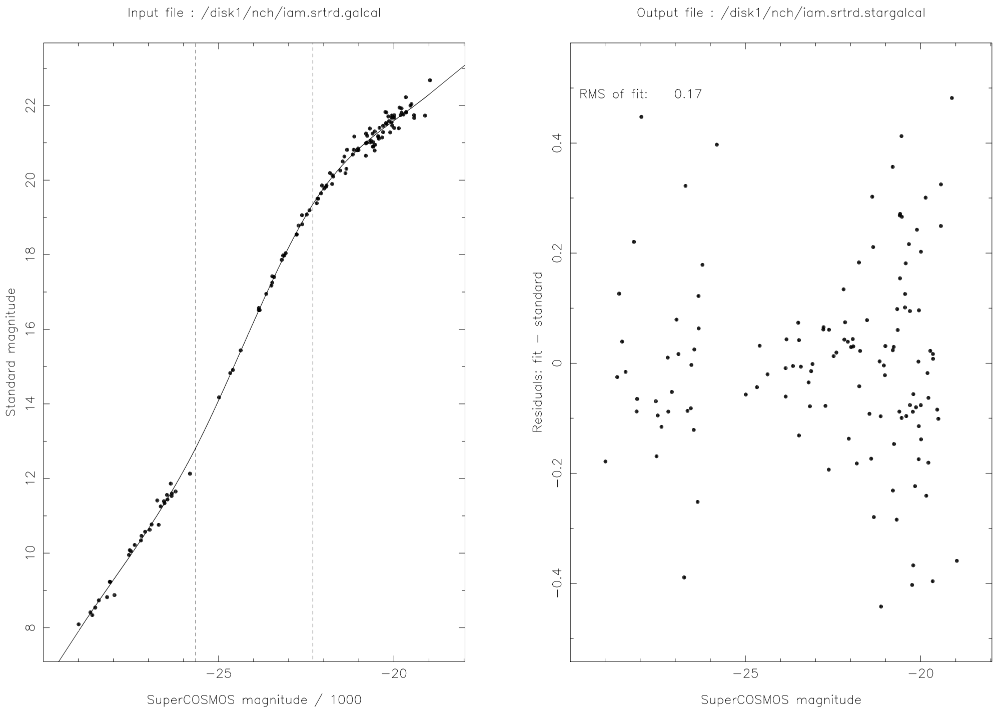

Figure 3: Output plot from code **starcal**. The left–hand panel shows the shape of the fitted least–squares cubic splines along with the data after iteration; the dashed lines indicate the position of the knots. The right–hand panel shows the residuals as a function of magnitude, and the overall RMS of the fit.

```
Calibrate stars only, or all images (reply s or a)?
s
Graphics device/type (? to see list, default xwindows):
xwindows
No. of calibrating stars input:     135
No. of calibrating stars used for fit:      128
No. of records read from input IAM file:   293222
No. of stars calibrated:     222519
%
```

A sky normalisation option is provided in `starcal` although in general it is *not* recommended to use this (see Section 6.2 for a more detailed discussion).

6 External accuracy of calibrated photographic data

Stone et al. (1996) describe an on–going project to provide deep astrometric standards using a CCD camera on a transit telescope. The data also provide accurate photometry down to V $\sim$ 18, and in this Section these photometric measurements are used to demonstrate some aspects of the external accuracy of the calibrated photographic magnitudes. The accuracy of the Stone data is estimated to be $\pm0.01^{\rm m}$ at R=10 rising to $\pm0.05^{\rm m}$ at R=18. The procedure outlined in the previous Section was used to calibrate all stars and galaxies in UKST survey field 891

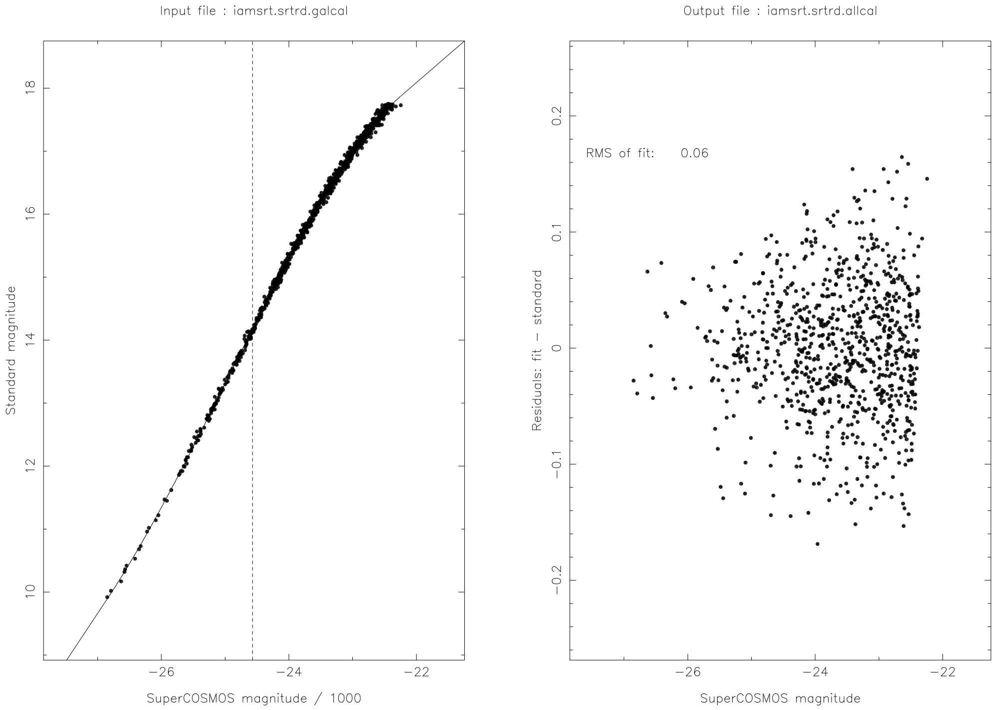

Figure 4: Stellar calibration of UKST plate OR12694 (survey field 891) using Stone photometric data.

on plate OR12694 (the second epoch 'AAO–R' survey plate). The Stone data run in a strip having a 3.5° range in DEC and covering the full RA range of the plate. To calibrate the entire plate, all objects within 0.5° of the plate centre were used to define the calibration curves (see Figures 4 and 5). Then, after having applied these calibrations to the whole plate, the residuals of tha calibrated photographic data versus the Stone data were examined as a function of plate position. This procedure simulates the calibration of an entire field based on sequence data near the plate centre (which is how most photoelectric sequence calibrations are achieved).

6.1 Photometric field effects

Figures 6 to 10 show the systematic trends in the residuals as a function of plate position when compared against the Stone data. Four magnitude slices for stars are shown indicating how the systematic errors increase for brighter images: typical errors are $< 0.1^{\mathrm{m}}$ at R=17.5 increasing to $> 0.2^{\mathrm{m}}$ at R=14.5. These errors are not well understood and change from plate to plate; furthermore they do not correlate well with any other image parameters (for example with sky level or with typical image shape which is sensitive to focus variation). It is probable that small variations in characteristic curve as a function of plate position coupled with the dynamic range limit of the machine are the source of this problem — stars brighter than 17^{th} magnitude will have peak diffuse densities > 4D on a deep sky survey plate, and SuperCOSMOS does not have sufficient dynamic range to penetrate such dense image cores. There is no way of correcting these position–dependent systematics other than doing a position–dependent calibration. In general the data required to do this will not be available, so no such code implementation is given here. Note also that there are no Stone data for comparisons in the extreme corners of the field, where vignetting effects are likely to be most significant. In summary, despite very low random

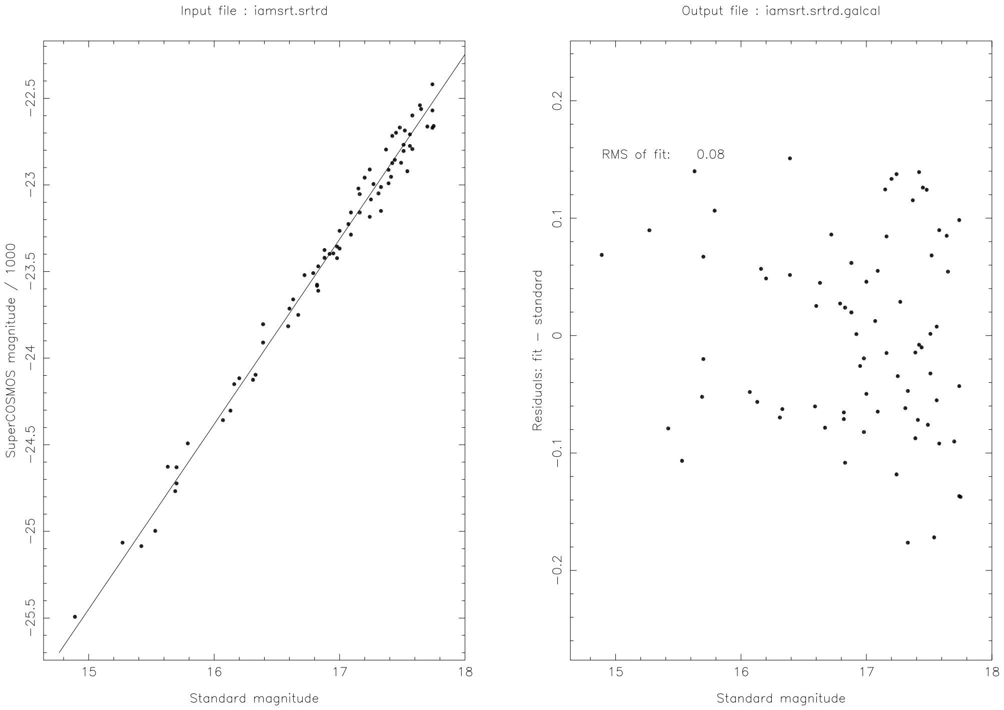

Figure 5: Galaxian calibration of UKST plate OR12694 (survey field 891) using Stone photometric data.

errors on small scales ($\sim 0.06^{\mathrm{m}}$ in Figure 4 for example) it should be noted that, depending on plate position and magnitude range, there can be large (*eg.* up to $\sim 0.2^{\mathrm{m}}$) systematic errors in calibrated photographic magnitudes due to variations in densitometric characteristics across the plate, particularly at the corners and edges.

6.2 Sky normalisation

In Figures 11 and 12 the stellar and galaxian calibration curves are shown for field 891, but this time the calibration has been done in terms of the sky background normalised instrumental magnitude versus standard magnitude. Small changes in these curves can be seen when compared with Figures 4 and 5; these differences are barely significant. However, the field effect comparison plots (Figures 13 and 14 respectively for stars and galaxies) show interesting differences when compared to those using un–normalised instrumental magnitudes (Figures 6 and 10). The galaxy field effects are significantly reduced, while for stars, although over most of the plate a small improvement in systematic residuals is perceptible, they are worse along the right–hand edge. In general, when working with deep sky survey plates sky normalisation is recommended for galaxy photometry. For stellar calibration it is probably better to use the instrumental magnitudes without normalisation to the sky level. Moreover, for short exposure plates having very low background levels, sky normalisation should never be used.

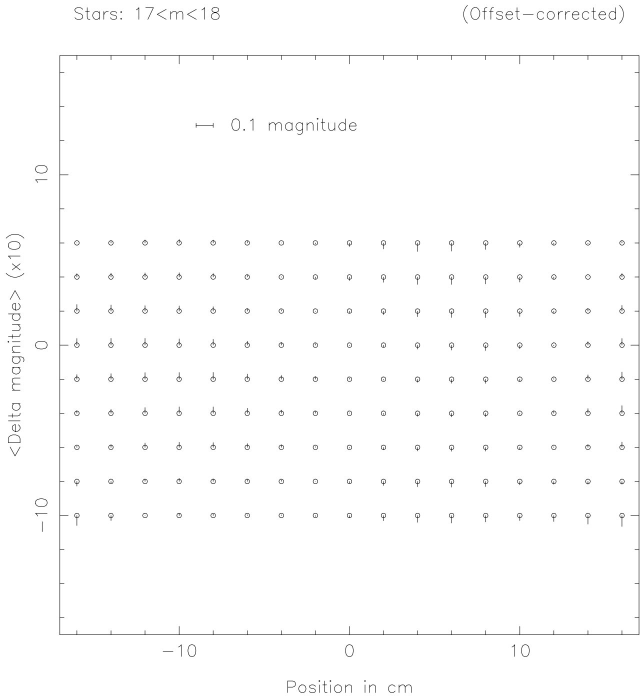

Figure 6: Systematics in calibrated stellar magnitudes in the range 17 < m < 18.

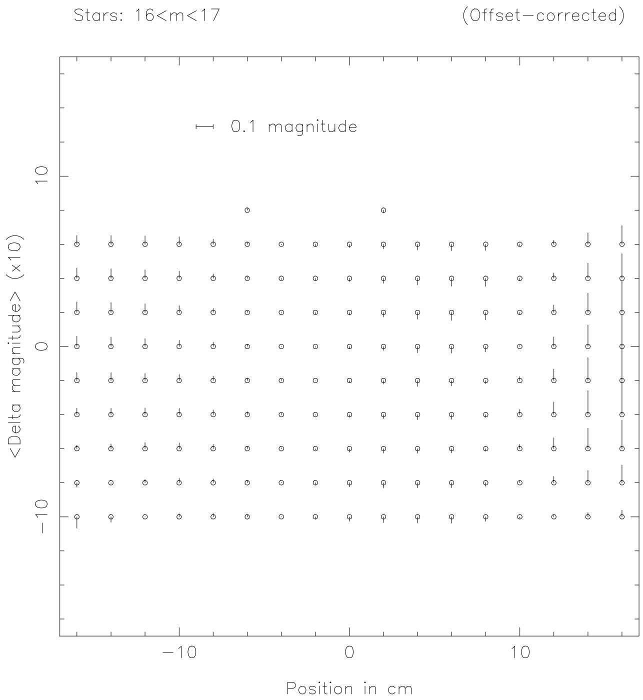

Figure 7: Systematics in calibrated stellar magnitudes in the range 16 < m < 17.

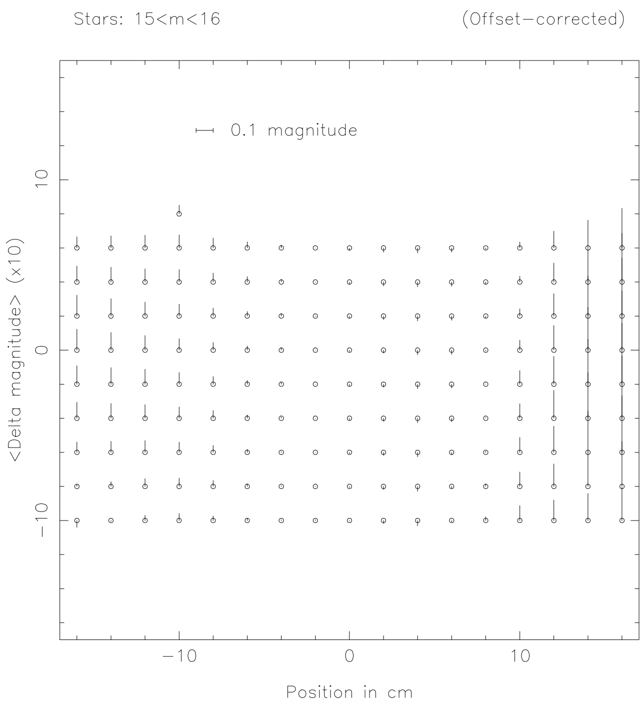

Figure 8: Systematics in calibrated stellar magnitudes in the range $15 < \mathrm{m} < 16$.

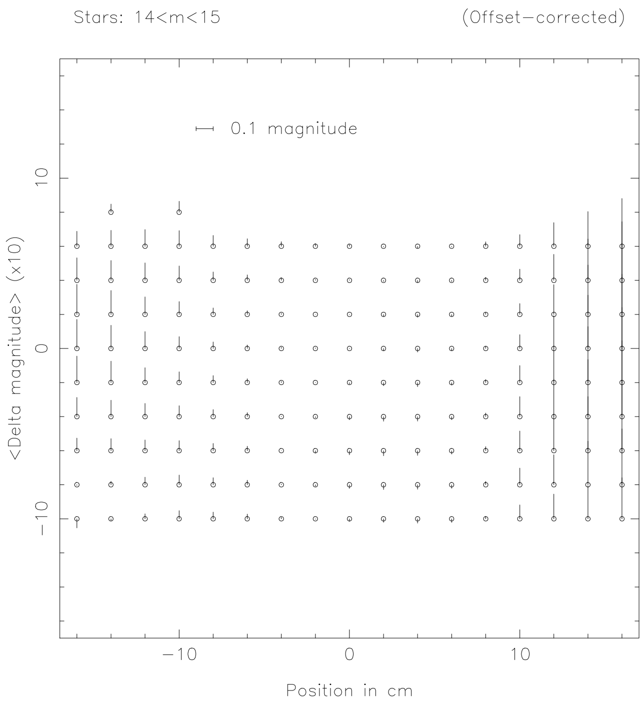

Figure 9: Systematics in calibrated stellar magnitudes in the range $14 < \mathrm{m} < 15$.

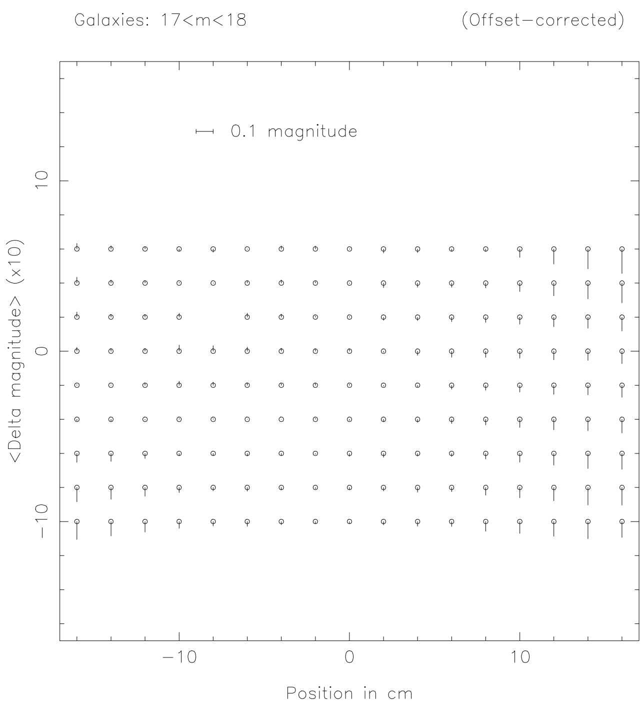

Figure 10: Systematics in calibrated galaxian magnitudes in the range $17 < m < 18$.

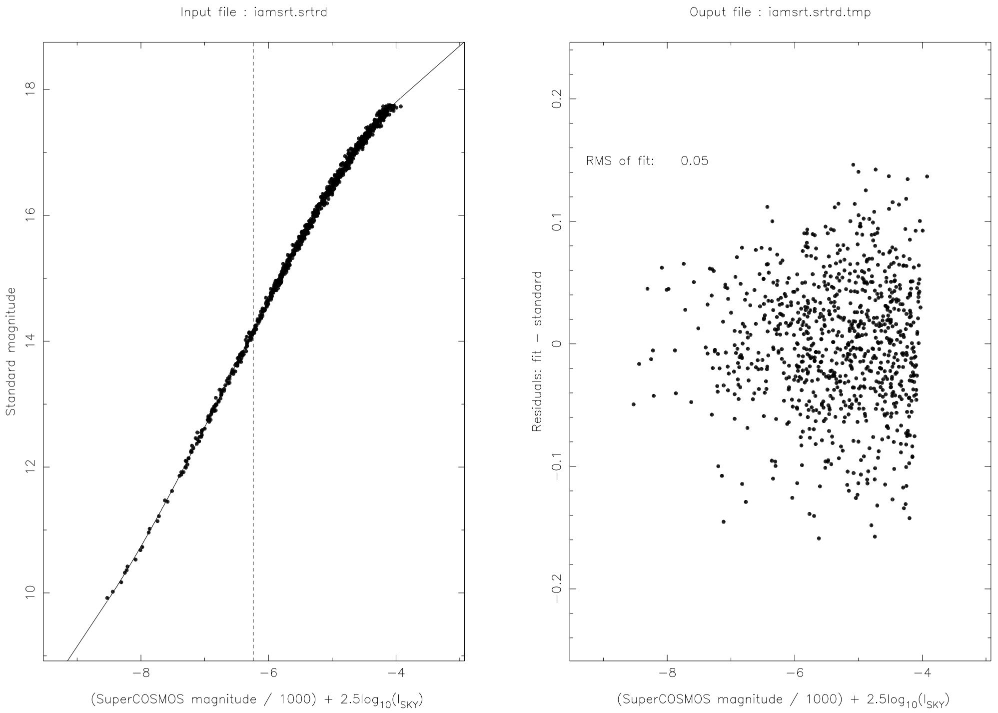

Figure 11: Stellar calibration of UKST plate OR12694 (survey field 891) using Stone photometric data and sky normalised instrumental magnitudes.

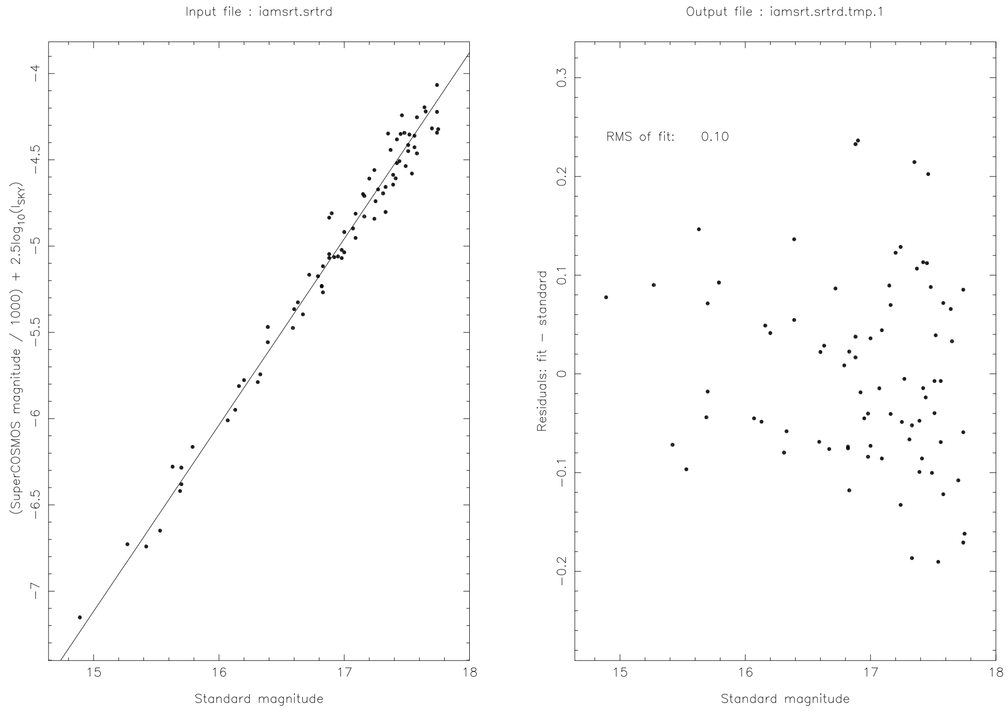

Figure 12: Galaxian calibration of UKST plate OR12694 (survey field 891) using Stone photometric data and sky normalised instrumental magnitudes.

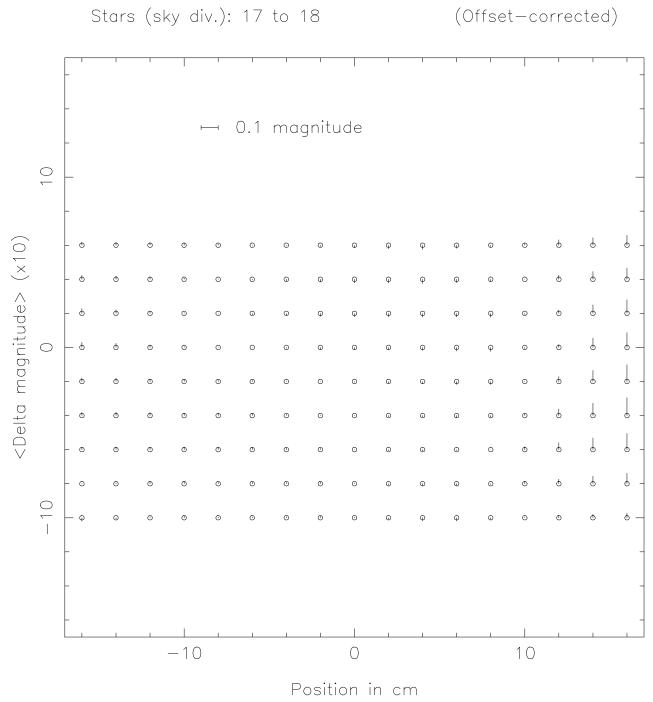

Figure 13: Systematics in calibrated galaxian magnitudes in the range $17 < \mathrm{m} < 18$.

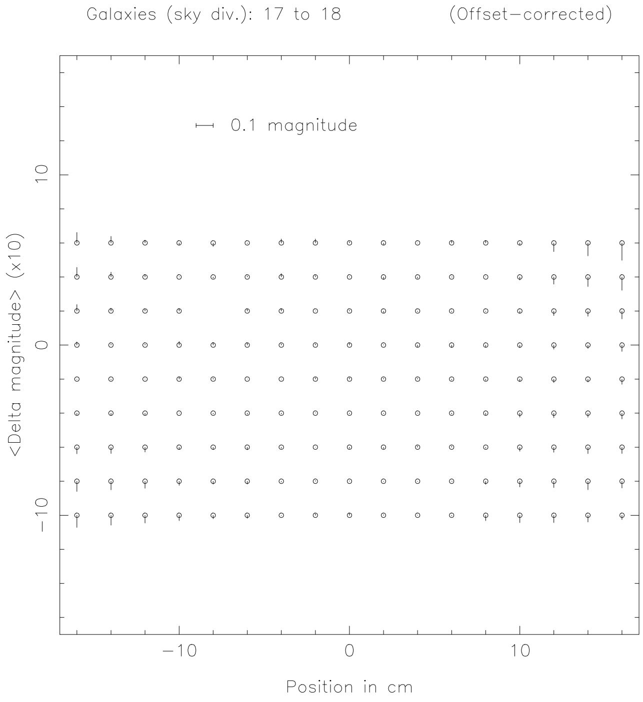

Figure 14: Systematics in calibrated galaxian magnitudes in the range 17 < m < 18.

7 Linearised instrumental magnitudes

Although there are several projects proposed or on–going to produce deep calibration sequences over the entire sky at 5° grid spacing for Schmidt survey calibration (*eg.* Maddox & Sutherland 1992; Postman et al. 1992; Boyle, Shanks & Croom 1995) data over the whole sky are not yet available. Since the SuperCOSMOS instrumental magnitude scale for stars is non–linear and not similar from plate to plate, it is difficult to estimate even approximate apparent magnitudes without a photoelectric sequence calibration. Bunclark & Irwin (1983) demonstrated a method of stellar magnitude linearisation based on areal profile invariance as a function of magnitude, allowing calibration using a few stars of known magnitude in each field along with an estimate of the depth of the scanned photograph.

Work is underway to implement stellar magnitude linearisation for SuperCOSMOS data. The relevant information will appear in this Section when it becomes available.

Acknowledgements

Thanks are due to Mike Irwin for many helpful discussions and for providing the code used to compare calibrated data against the Stone standards. We are grateful to Ron Stone for supplying unpublished data in electronic form for the comparison tests.

References

Bessell M.S., 1979, PASP, 91, 589
Bessell M.S., 19869, PASP, 98, 1303
Blair M., Gilmore G., 1982, PASP, 94, 742
Boyle B.J., Shanks T., Croom S.M., 1995, MNRAS, 276, 33
Bunclark P.S., Irwin M.J., 1983, In: Proc. Statistical Methods in Astromony Symp., ESA SP–201
Evans D.W., 1989, A&AS, 78, 249
Hatzidimitriou D., Hawkins M.R.S., Gyldenkerne K., 1989, MNRAS, 241, 645
James T.H. (ed.), 1977, 'The Theory of the Photographic Process', Macmillan.
Maddox S.J., Sutherland W.J., 1992, In: Digitised Optical Sky Surveys, Eds. H.T. MacGillivray & E.B. Thomson, Kluwer, 53
Metcalfe N., Fong R., Shanks T., 1995, MNRAS, 274, 769
Postman M., Siciliano L., Shara M., Rehner D., Brosch N., Struch C., Bucciarelli B., Lopez C., 1992, In: Digitised Optical Sky Surveys, Eds. H.T. MacGillivray & E.B. Thomson, Kluwer, 61
Stone R.C., Monet D.G., Monet A.K.B., Walker R.L., Ables H.D., Bird A.R., Harris F.H., 1996, AJ, 111, 1721
Tritton S.B., 1983, 'The United Kingdom Schmidt Telescope Handbook', Royal Observatory Edinburgh